Exciton Transport in Suspended Single Carbon Nanotubes Studied by Photoluminescence Imaging Spectroscopy

Kohei Yoshikawa,[†] Kazunari Matsuda,*[,†] and Yoshihiko Kanemitsu[†,‡]

Institute for Chemical Research, Kyoto University, Uji, Kyoto 611-0011, Japan, and Photonics and Electronics Science and Engineering Center, Kyoto University, Kyoto 615-8510, Japan

Received: December 4, 2009; Revised Manuscript Received: January 23, 2010

We studied the spatial profiles and time traces of the photoluminescence (PL) intensity of suspended single-walled carbon nanotubes (SWNTs) using a microscopic PL imaging technique. These PL images, obtained in different gases, showed that adsorbed oxygen molecules act as PL quenchers in SWNTs. The exciton transport length of suspended SWNTs was estimated to be ~200 nm at room temperature. We found that the exciton transport and its temperature dependence are dominated by the diffusive motion of a one-dimensional exciton in a single carbon nanotube.

Introduction

The optical properties of single-walled carbon nanotubes (SWNTs) are intensively studied from the viewpoint of fundamental physics[1] and for their potential applications in optoelectronic devices such as electroluminescence[2] and single photon sources.[3] Because the excited electrons and holes are strongly confined in the one-dimensional (1D) materials, the correlated electron−hole pairs form stable 1D excitons with the extremely large binding energies on the order of several hundred meV.[4−9] Both the temporal and the spatial dynamics of 1D excitons determine the optical properties of the SWNTs. Many experimental efforts have been devoted to reveal the temporal dynamics of excitons using time-resolved optical spectroscopy.[10−13]

So far, there are a few studies that are concerned with the spatial dynamics of excitons in the SWNTs using PL imaging spectroscopy.[14,15] Although the spatial dynamics of excitons plays important roles in the characteristic optical properties in SWNTs, such as the extraordinary sensitivity of photoluminescence (PL) against the local environment,[14] and nanotube length-dependent PL quantum yield,[16] the understanding of the exciton transport does not progress, and the measured exciton transport lengths during its recombination lifetime vary from ~10 to ~90 nm.[14,17] Moreover, the detailed mechanism of the exciton transport, whether the exciton motion can be treated as diffusive or not, is the issue under intense debate.[14] Therefore, it is necessary to elucidate the exciton transport for understanding the optical properties of SWNTs.

We studied the exciton transport length and its temperature dependence in as-grown single carbon nanotubes using microscopic PL spectroscopy. Time traces of the PL intensity in different atmospheres reveal that oxygen molecule adsorption introduces nonradiative recombination centers for excitons in SWNTs. From the change of the PL spatial profiles, we estimated a room-temperature exciton diffusion length of ~200 nm. Moreover, we discussed the detailed mechanism of exciton diffusion.

* To whom correspondence should be addressed. E-mail: matsuda@scl.kyoto-u.ac.jp.
[†] Institute for Chemical Research.
[‡] Photonics and Electronics Science and Engineering Center.

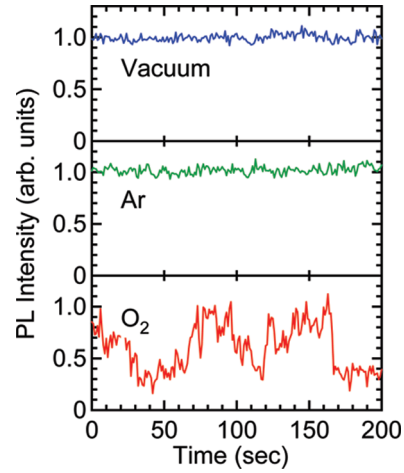

Figure 1. Time traces of PL intensity of (7,5) SWNT in different atmospheres. Vacuum results were at 10^{-3} Torr; Ar and O_2 results were at 760 Torr.

Experimental Section

Sample Preparation. The SWNTs were grown directly on Si or SiO_2 substrates using the catalytic-chemical vapor-deposition method.[18] The substrates were patterned with parallel grooves with widths varying from 350 nm to 10 μm and depths from 1 to 3 μm. The Co/Mo acetic acetates in the methanol used for the catalysts were dispersed on the substrates with a spin-coating technique. The SWNTs, grown at 900 °C for 10 min, were suspended across the grooves and were isolated from one another.[19−21]

Measurements. The PL imaging is one of the powerful methods to study the exciton transport[14,15] and was done using a cryostat-equipped home-built microscope where the temperature and gas atmosphere of the sample were varied in the cryostat. An objective (100×, 0.8 NA) was used for the PL imaging, with a 1.96 eV He−Ne laser used for excitation of the sample. The excitation spot diameter and density were about 35 μm and ~200 W/cm^2, respectively. The PL signals from the SWNTs were detected with an electron-multiplying charge-coupled device camera through a long-wave pass filter (>950 nm). The PL imaging spatial resolution was ~900 nm.

10.1021/jp911518h © 2010 American Chemical Society
Published on Web 02/18/2010

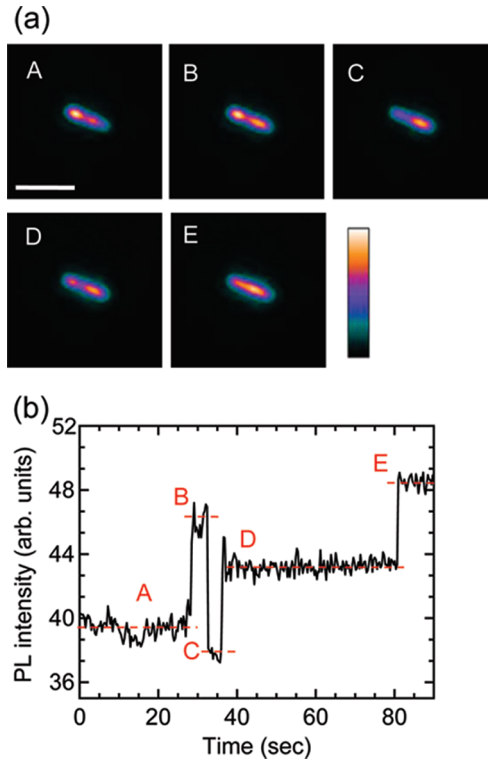

Figure 2. (a) Sequential PL images at each time stamp (A−E). The scale bar in the PL image (A) corresponds to 5 μm. (b) Time trace of PL intensity for an ~3 μm long SWNT at room temperature in air. The A−E time stamp is indicated in the figure.

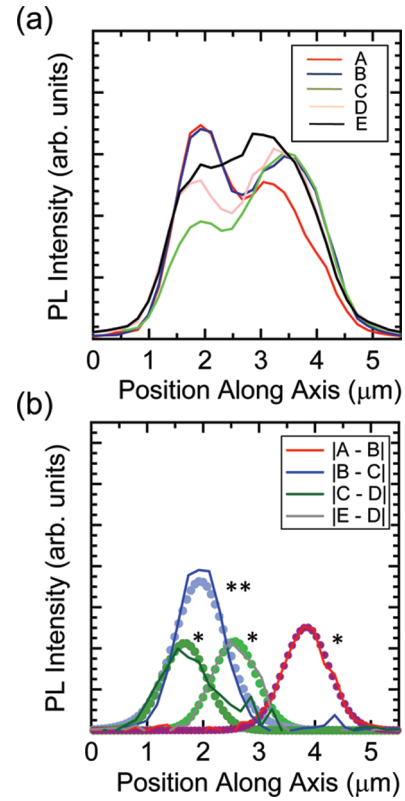

Figure 3. (a) PL spatial profiles of ~3 μm long SWNTs along the nanotube axis. Each index (A−E) corresponds to the time stamps in Figure 2a and b. (b) Differential PL spatial profiles. The number of oxygen molecules adsorbed is indicated by asterisks. Solid lines show experimental results; solid dots show the calculated differential PL profiles.

Results and Discussion

Figure 1 shows PL intensity time traces of a (7,5) single carbon nanotube at room temperature in vacuum, Ar, and O_2 atmospheres, respectively. The PL intensities are stable and maintain almost constant values in vacuum and Ar atmospheres. In these vacuum and Ar atmospheres, the laser light irradiation does not create PL quenching centers such as photoinduced defects and/or locally ionized states,[22] and thus does not affect the PL intensity. In contrast, in the O_2 atmosphere, the PL intensity randomly fluctuates and shows discrete changes. This large PL intensity fluctuation in O_2 comes from the adsorption and desorption of oxygen molecules on the SWNT sidewall where the adsorbed oxygen molecules act as electron acceptors,[23−25] and locally doped holes quench the PL intensity via exciton−hole nonradiative recombination processes.[26]

Figure 2a shows temporal PL image sequences of an ~3 μm long, single carbon nanotube at room temperature in air. The elongated PL images reflect the observation of nanotubes longer than the optical microscopy spatial resolution (~900 nm). Moreover, as will be discussed below, the PL intensity is spatially inhomogeneous, and the intensity profile changes as time proceeds (A−E). Figure 2b shows the time trace of the spatially integrated PL intensity over the whole nanotube length. The time trace in Figure 2b clearly shows that the PL intensity changes discretely. Because of the difference in the nanotube length, the relative amplitude of the PL intensity changes for a single step is smaller than that in Figure 1.

Figure 3a shows spatial profiles of PL images along a nanotube axis at each time stamp (A−E) in Figure 2a. One can see the spatially inhomogeneous profiles and the changes in the intensity as time proceeds. We evaluated the differential profiles in Figure 3b to analyze the spatial- and time-dependent PL intensity. The differential profiles show positive and negative peaks corresponding to the adsorption and desorption of oxygen molecules on the carbon nanotube sidewall. Note that the absolute amplitude of the peaks in the differential profiles shows discrete rather than continuous values. This experimental result indicates that both the desorption and the adsorption of small numbers of oxygen molecules, indicated by the asterisks in the figure, contribute to the PL intensity profile changes.

The excitons are generated uniformly throughout the nanotube by a large photoexcitation spot in the optical microscope. The generated excitons near the oxygen adsorption site recombine nonradiatively very fast. As a result, the PL intensity near the oxygen adsorbing site within the exciton transport length is very low in comparison with the other parts in a SWNT, and the oxygen adsorbing site becomes a PL quenching spot in the image.[14] Thus, the PL quenching size along the nanotube axis contains information on the exciton transport length.

The differential PL intensity profiles can be used to derive the exciton transport length to the quenching site. Taking into account a single PL quenching site, the differential profiles $\Delta I(x)$ in Figure 3b can be expressed from the diffusion equation as[27−29]

$$\Delta I(x) = A \exp\left(-\frac{|x - x_1|}{L}\right) \quad (1)$$

where A is the PL intensity per SWNT unit length and x_1 is the adsorbed position of the oxygen molecule. A is determined from the highest intensity in the spatial profiles. As the spatial resolution of the optical microscopy broadens the differential PL intensity profiles, the instrumental response function was convoluted with the PL quenching spatial profiles in eq 1 to

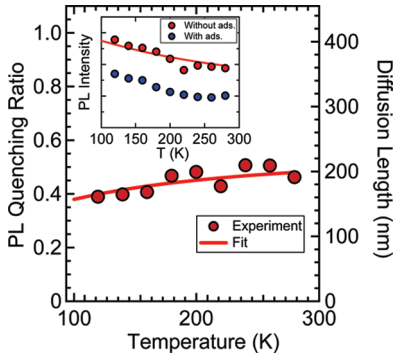

Figure 4. Temperature dependence of PL quenching ratio defined as $\Delta I_{PL} = (I_{PL}' - I_{PL})/I'_{PL}$. The solid line shows the calculated result using eq 5. The inset shows the temperature dependence of the PL intensity of a single nanotube with and without oxygen adsorption. The solid line shows the curve fitted by the $(\sqrt{T})^{-1}$ function.

calculate the differential PL intensity profiles shown as circles in Figure 3b. These calculated differential PL profiles agree well with the experimental results. The exciton transport length L_d is calculated from the full width at half-maximum (fwhm: $2L$ ln 2) of the calculated profiles. We also measured the PL images of five different (7,5) single carbon nanotube with lengths longer than 2 μm and estimated the exciton transport lengths using the same procedure. The exciton transport lengths were typically 170−240 nm, with an average of 200 nm. The exciton transport length of about 200 nm in the suspended SWNTs is not inconsistent with the values in the micelle-encapsulated SWNTs in refs 14 and 15, considering the difference of PL lifetimes.[13,30] The derived exciton transport length of about 200 nm is not negligibly short as compared to a typical nanotube length (~1 μm), indicating that even a single oxygen molecule adsorption on the sidewall of a SWNT strongly affects the PL intensity.

To understand the exciton transport mechanism, we also studied the PL intensity temperature dependence. The inset of Figure 4 presents the temperature dependence for the same ~1 μm long single carbon nanotube with and without oxygen molecule adsorption. From the relative PL intensity amplitude change with the adsorption of oxygen molecules at 280 K, the number of PL quenching centers can be estimated in the single carbon nanotube. The PL intensity of a single carbon nanotube, without oxygen molecule adsorption, gradually increases from 280 to around 100 K with a maximum value at 60 K, and it decreases below 60 K. This characteristic temperature dependence of the PL intensity is determined by the radiative lifetime of the 1D exciton as a $(\sqrt{T})^{-1}$ due to thermalization in the bright exciton band[31] and by the exciton distribution between the bright and dark states that have a splitting energy of 5 meV.[32,33] The solid line in the inset of Figure 4 above 100 K shows the $(\sqrt{T})^{-1}$ dependence of the PL intensity, as expected from the 1D exciton behavior, and fits the experimental results well. However, the PL intensity below 100 K is complicated because of the dark exciton state contribution. Therefore, we henceforth limit our study of the experimental results to the regime above 100 K where the PL behavior is simply determined by the 1D bright exciton dynamics.

The PL intensity temperature dependence for a single carbon nanotube with quenching centers is described as

$$I_{PL}(T) \propto A(T) \int_0^l \left[1 - \sum_{i=1}^{N} \exp\left(-\frac{|x - x_i|}{L(T)}\right)\right] dx \quad (2)$$

where N is the number of additional PL quenching center due to the adsorption of oxygen molecule, x_i is the position of oxygen adsorption site, and l is a nanotube length. $A(T)$ in eq 2 includes the various temperature-dependent factors, such as the radiative exciton recombination rate, and exciton population between the bright and dark states as discussed above, and can be canceled out by using the normalized differential PL intensity ΔI_{PL} with and without oxygen adsorption. For $l > L$ and $L < x_i < l-L$, ΔI_{PL} is described as

$$\Delta I_{PL} = (I'_{PL} - I_{PL})/I'_{PL} \quad (3)$$

where I'_{PL} and I_{PL} are the PL intensities without and with oxygen adsorption, respectively. Because ΔI_{PL} is approximately proportional to $L_d(T)$, we can derive the temperature-dependent exciton transport length from ΔI_{PL}. Figure 4 shows the temperature dependence of the normalized differential PL intensity defined as the PL quenching ratio. The exciton transport length, normalized by the value at 300 K, is also plotted as a function of temperature. The normalized differential PL intensity decreases slightly with decreasing temperature, indicating the slight shortening of the exciton transport length in the low temperature region.

To discuss the mechanism of the exciton transport and its temperature dependence, we consider the diffusive exciton transport. The exciton diffusion length is described as[14,27,34]

$$L_d(T) = \sqrt{2D\langle\tau_{ex}\rangle} \quad (4)$$

where D ($= k_B T\langle\tau_{scat}\rangle/M$) is a diffusion constant using the Einstein relation, $\langle\tau_{scat}\rangle$ is an exciton scattering time, M is an exciton center of mass, and $\langle\tau_{ex}\rangle$ is an exciton lifetime. Both $\langle\tau_{ex}\rangle$ and $\langle\tau_{scat}\rangle$ could contribute to the temperature dependence of the diffusion length. The $\langle\tau_{ex}\rangle$ corresponding to the PL lifetime determined by the nonradiative exciton recombination process is almost constant as a function of temperature above 100 K.[13] In this temperature range, the exciton scattering process is mainly determined by the low energy acoustic phonon and defects and/or impurities.[35] The exciton scattering rate is described as

$$\langle\tau_{sctt}\rangle^{-1} \propto A_{ph}T + \Gamma_0 \quad (5)$$

where A_{ph} is a coefficient of exciton−acoustic phonon interaction and Γ_0 is an exciton−impurity/defect scattering term.[36−39] The solid line in Figure 4 shows the calculated exciton diffusion length from eqs 4 and 5 using the values $A_{ph} = 0.035$ meV/K and $\Gamma_0 = 5$ meV. The calculated line fits the experimental result for the temperature dependence of the exciton diffusion length well. Moreover, the values of A_{ph} and Γ_0 are reasonably consistent with those from experimental results for homogeneous linewidths.[39] Thus, we conclude that the exciton transport and its temperature dependence are dominated by the diffusive motion of 1D excitons in SWNTs.

Conclusions

We studied the exciton transport of a suspended SWNT by combining PL imaging and oxygen molecule adsorption experiments. We estimated the exciton diffusion length of about 200 nm at room temperature and found that it decreased slightly with decreasing temperature. This evaluated diffusion length

of 200 nm is not negligibly short as compared to a typical nanotube length of ~1 μm, and it affects the PL intensity and its temperature dependence. These exciton diffusion dynamics results provide us with important insight into the optical properties of SWNTs.

Acknowledgment. We thank H. Suzuura, Y. Miyauchi, and R. Matsunaga for helpful discussions, and S. Kasai and T. Ono for technical support in fabricating the grooved Si substrates. This study was supported by a Grant-in-Aid for Scientific Research from JSPS (no. 20340075) and from MEXT of Japan (nos. 20048004 and 20104006).

References and Notes

(1) Saito, R.; Dresselhaus, G.; Dresselhaus, M. S. *Physical Properties of Carbon Nanotubes*; Imperial College Press: London, 1998.
(2) Chen, J.; Perebeinos, V.; Freitag, M.; Tsang, J.; Fu, Q.; Liu, J.; Avouris, P. *Science* **2005**, *310*, 1171.
(3) Högele, A.; Galland, C.; Winger, M.; Imamoğlu, A. *Phys. Rev. Lett.* **2008**, *100*, 217401.
(4) Ando, T. *J. Phys. Soc. Jpn.* **1997**, *66*, 1066.
(5) Zhao, H.; Mazumdar, S. *Phys. Rev. Lett.* **2004**, *93*, 157402.
(6) Perebeinos, V.; Tersoff, J.; Avouris, Ph. *Nano Lett.* **2005**, *5*, 2495.
(7) Spataru, C. D.; Ismail-Beigi, S.; Capaz, R. B.; Louie, S. G. *Phys. Rev. Lett.* **2005**, *95*, 247402.
(8) Wang, F.; Dukovic, G.; Brus, L. E.; Heinz, T. F. *Science* **2005**, *308*, 838.
(9) Maultzsch, J.; Pomraenke, R.; Reich, S.; Chang, E.; Prezzi, D.; Ruini, A.; Molinari, E.; Strano, M. S.; Thomsen, C.; Lienau, C. *Phys. Rev. B* **2005**, *72*, 241402(R).
(10) Wang, F.; Dukovic, G.; Brus, L. E.; Heinz, T. F. *Phys. Rev. Lett.* **2004**, *92*, 177401.
(11) Ostojic, G. N.; Zaric, S.; Kono, J.; Strano, M. S.; Moore, V. C.; Hauge, R. H.; Smalley, R. E. *Phys. Rev. Lett.* **2004**, *92*, 117402.
(12) Jones, M.; Engtrakul, C.; Metzger, W. K.; Ellingson, R. J.; Nozik, A. J.; Heben, M. J.; Rumbles, G. *Phys. Rev. B* **2005**, *71*, 115426.
(13) Hirori, H.; Matsuda, K.; Miyauchi, Y.; Maruyama, S.; Kanemitsu, Y. *Phys. Rev. Lett.* **2006**, *97*, 257401.
(14) Cognet, L.; Tsyboulski, D.; Rocha, J.; Doyle, C.; Tour, J.; Weisman, R. *Science* **2007**, *316*, 1465.
(15) Qian, H.; Georgi, C.; Anderson, N.; Green, A. A.; Hersam, M. C.; Novotny, L.; Hartschuh, A. *Phys. Status Solidi B* **2009**, *245*, 2243.
(16) Heller, D. A.; Mayrhofer, R. M.; Baik, S.; Grinkova, Y. V.; Usrey, M. L.; Strano, M. S. *J. Am. Chem. Soc.* **2004**, *126*, 14567.
(17) Luer, L.; Hoseinkhani, S.; Polli, D.; Crochet, J.; Hertel, T.; Lanzani, G. *Nature Phys.* **2008**, *5*, 54.
(18) Maruyama, S.; Kojima, R.; Miyauchi, Y.; Chiashi, S.; Kohno, M. *Chem. Phys. Lett.* **2002**, *360*, 229.
(19) Lefebvre, J.; Homma, Y.; Finnie, P. *J. Phys. Chem. C* **2009**, *113*, 7536.
(20) Lefebvre, J.; Austing, D. G.; Bond, J.; Finnie, P. *Nano Lett.* **2006**, *6*, 1603.
(21) Inoue, T.; Matsuda, K.; Murakami, Y.; Maruyama, S.; Kanemitsu, Y. *Phys. Rev. B* **2006**, *73*, 233401.
(22) Harutyunyan, H.; Gokus, T.; Green, A. A.; Hersam, M. C.; Allegrini, M.; Hartschuh, A. *Nano Lett.* **2009**, *9*, 2010.
(23) Dukovic, G.; White, B.; Zhou, Z.; Wang, F.; Jockusch, S.; Steigerwald, M.; Heinz, T.; Friesner, R.; Turro, N.; Brus, L. *J. Am. Chem. Soc.* **2004**, *126*, 15269.
(24) Jhi, S.-H.; Louie, S. G.; Cohen, M. L. *Phys. Rev. Lett.* **2000**, *85*, 1710.
(25) Lebedkin, S.; Kareev, I.; Hennrich, F.; Kappes, M. M. *J. Phys. Chem. C* **2008**, *112*, 16236.
(26) Perebeinos, V.; Avouris, P. *Phys. Rev. Lett.* **2008**, *101*, 057401.
(27) Richter, A,; Behme, G.; Süptitz, M.; Lienau, Ch.; Elsaesser, T.; Ramsteiner, M.; Nötzel, R.; Ploog, K. H. *Phys. Rev. Lett.* **1997**, *79*, 2145.
(28) Hillmer, H.; Forchel, A.; Hansmann, S.; Morohashi, M.; Lopez, E.; Meier, H. P.; Ploog, K. *Phys. Rev. B* **1989**, *39*, 10901.
(29) Rajan, A.; Strano, M. S.; Heller, D. A.; Hertel, T.; Schulten, K. *J. Phys. Chem. B* **2008**, *112*, 6211.
(30) Xiao, Y.-F.; Nhan, T. Q.; Wilson, M. W. B.; Fraser, J. M. *Phys. Rev. Lett.* **2010**, *104*, 017401.
(31) Mortimer, I. B.; Nicholas, R. J. *Phys. Rev. Lett.* **2007**, *98*, 027404.
(32) Matsunaga, R.; Matsuda, K.; Kanemitsu, Y. *Phys. Rev. Lett.* **2008**, *101*, 147404.
(33) Srivastava, A.; Htoon, H.; Klimov, V. I.; Kono, J. *Phys. Rev. Lett.* **2008**, *101*, 087402.
(34) Nagamune, Y.; Watabe, H.; Sogawa, F.; Arakawa, Y. *Appl. Phys. Lett.* **1995**, *67*, 1535.
(35) Suzuura, H.; Ando, T. *Phys. Rev. B* **2002**, *65*, 235412.
(36) Matsuda, K.; Inoue, T.; Murakami, Y.; Maruyama, S.; Kanemitsu, Y. *Phys. Rev. B* **2008**, *77*, 033406.
(37) Graham, M.; Ma, Y.-Z.; Fleming, G.-R. *Nano Lett.* **2008**, *8*, 3936.
(38) Ichida, M.; Kiyohara, Y.; Saito, S.; Miyata, Y.; Kataura, H.; Ando, H. *Phys. Status Solidi B* **2008**, *245*, 2712.
(39) Yoshikawa, K.; Matsunaga, R.; Matsuda, K.; Kanemitsu, Y. *Appl. Phys. Lett.* **2009**, *94*, 093109.

JP911518H